2004

Development of First Principles Capacity Fade Model for Li-Ion Cells

P. Ramadass
University of South Carolina - Columbia

Bala Haran
University of South Carolina - Columbia

Parthasarathy M. Gomadam
University of South Carolina - Columbia

Ralph E. White
University of South Carolina - Columbia, white@cec.sc.edu

Branko N. Popov
University of South Carolina - Columbia, popov@engr.sc.edu

Publication Info

Journal of the Electrochemical Society, 2004, pages A196-A203.

Journal of The Electrochemical Society, **151** (2) A196-A203 (2004)
0013-4651/2004/151(2)/A196/8/$7.00 © The Electrochemical Society, Inc.

Development of First Principles Capacity Fade Model for Li-Ion Cells

P. Ramadass,* Bala Haran, Parthasarathy M. Gomadam,* Ralph White,*** and Branko N. Popov**,z**

Department of Chemical Engineering, University of South Carolina, Columbia, South Carolina 29208, USA

A first principles-based model has been developed to simulate the capacity fade of Li-ion batteries. Incorporation of a continuous occurrence of the solvent reduction reaction during constant current and constant voltage (CC-CV) charging explains the capacity fade of the battery. The effect of parameters such as end of charge voltage and depth of discharge, the film resistance, the exchange current density, and the over voltage of the parasitic reaction on the capacity fade and battery performance were studied qualitatively. The parameters that were updated for every cycle as a result of the side reaction were state-of-charge of the electrode materials and the film resistance, both estimated at the end of CC-CV charging. The effect of rate of solvent reduction reaction and the conductivity of the film formed were also studied.
 [DOI: 10.1149/1.1634273]

Manuscript submitted May 4, 2003; revised manuscript received July 30, 2003. Available electronically January 8, 2004.

In this study, an attempt was made to develop a first principles capacity fade model for Li-ion batteries. Darling and Newman[1] made a first attempt to model the parasitic reactions in lithium batteries by incorporating a solvent oxidation side reaction into a lithium-ion battery model. The model explains the self-discharge process occurring in Li-ion cells. Recently, Spotnitz[2] developed polynomial expressions for estimation of irreversible and reversible capacity losses due to solid electrolyte interphase (SEI) growth and dissolution. According to the author the expressions were difficult to use in conjunction with time temperature superposition. Also, the model requires extensive experimental cycling data to resolve the model parameters.

Side reactions and degradation processes in lithium-ion batteries may cause a number of undesirable effects leading to capacity loss.[3] If the cyclable lithium in the cell is reduced due to side reactions of any type, the capacity balance is changed irreversibly and the degree of lithium insertion in both electrodes during cell cycling is changed. The objective of this paper was to develop a capacity fade model through incorporation of side reactions with the existing Li-ion intercalation model.

Model Development

The side reaction of general interest in lithium-ion batteries is passive film formation on the negative electrode. The reduction reactions taking place which lead to the deposition of solid products are less understood, large in number, and varied in their nature depending on the composition of the electrolyte solution.[3] Thus to develop the model, the side reaction should be considered as consumption of solvent species and Li ions to form a group of such as: Li-alkyl carbonates, Li_2CO_3, etc., based on the composition and concentration of solvent. Similar to semiempirical capacity fade models developed earlier,[4] only the negative electrode was considered for developing a simplified first principles capacity fade model.

The solvent diffusion model developed for Li-ion cells under storage[5] explains the aging mechanism and helps to predict the calendar life. The model was based upon diffusion of the organic solvent present in the battery electrolyte followed by reduction near the negative electrode surface thereby forming unwanted products which form as a passive film (SEI). Previous studies of the SEI on lithiated carbon, both theoretical[6-8] and experimental,[9] have recognized that the film may have a significant porosity. Thus the mechanism for SEI growth as a result of solvent diffusion through the SEI seems plausible.

According to Aurbach *et al.*,[10] Li-ion insertion into graphite particles during charging causes increase in lattice volume due to an increase in the space between the graphene planes. Change in volume leads to stretching of the surface films on the edge planes through which Li ions are inserted into the graphite. It is well known that the surface film, usually comprised of a mixture of Li salts (both organic and inorganic), has a limited flexibility. Accordingly, one can expect the surface film to break during the Li-ion insertion reaction due to increase in particle volume, which alters the film passivity and exposes more of the underlying carbon to the electrolyte.

This phenomenon supports our assumption that continuous small-scale reactions occur between the lithiated carbon and solvent species, which increase the surface impedance with cycling. Also, the same process explains the large increase of the electrode impedance at higher temperatures, which is attributed to the increased rate of the repeated film formation.

The first principles capacity fade model developed here is based on a continuous occurrence of a very slow solvent diffusion/reduction near the surface of the negative electrode in case when the cell is in charge mode (both constant current and constant voltage charging). In other words, loss of the active material with continuous cycling was attributed to a continuous film formation over the surface of the negative electrode.

Choice of side reaction and assumptions.—

1. There are several possible reaction mechanisms between lithiated carbon and the electrolyte solution. The nature of the reaction depends upon the type of solvent mixture used in the battery electrolyte. Possible contaminants in the system include gases such as: CO_2, O_2, and N_2. Since most of the Li-ion systems use ethylene carbonate (EC) as one of the organic solvent for the electrolyte, the simplest reaction scheme that can be considered for modeling capacity loss is the reduction of EC. The reaction can be expressed as

$$S + 2Li^+ + 2e^- \rightarrow P \qquad [1]$$

where S refers to the solvent and P is the product formed as a result of side reaction.

2. The solvent reduction reaction occurs only during charging the Li-ion cell and it occurs during both constant current and constant voltage charging. Because the ratio of charge to discharge capacity remains close to 100%, it would be a valid assumption not to consider any side reaction or capacity fade during discharge.

3. The products formed as a result of side reaction (EC reduction) may be a mixture of organic and inorganic Li-based compounds and not Li_2CO_3 alone. The reason behind this is that, if we consider the entire product formed as lithium carbonate, it would result in overestimation of film resistance with cycling because it is a very poor conductor. Thus in order to obtain better predictions for discharge performance both in terms of decrease in capacity as well

* Electrochemical Society Student Member.
** Electrochemical Society Active Member.
*** Electrochemical Society Fellow.
z E-mail: popov@engr.sc.edu

as increase in cell resistance, we assume that a mixture of products of reasonable conductivity would be formed as a result of solvent reduction.

4. The side reaction is assumed to be irreversible and a value of 0.4 V *vs.* Li/Li^{+}[10,11] has been chosen as the open circuit potential for the solvent reduction reaction.

5. The initial resistance of the SEI formed during the formation period was taken as 100 Ω cm^2.

6. To make the model simpler, no overcharging conditions have been considered thereby the other side reaction, namely lithium deposition, could be eliminated.

Interfacial reaction kinetics.—For the semi-empirical model,[4] the Butler-Volmer (BV) kinetic expression was used to describe the overall charge transfer process occurring across the electrode/electrolyte interfaces. In this model BV kinetics was defined separately for Li-ion intercalation reaction[12-15] and for the solvent reduction reaction. Thus, for the negative electrode, the local volumetric charge transfer current density was defined as the summation of intercalation and side reaction current densities which is given by

$$J = J_1 + J_s \quad [2]$$

BV kinetics for Li-ion intercalation reaction.—The local volumetric transfer current density due to Li-ion intercalation occurring across both electrode/electrolyte interfaces is given by

$$J_1 = a_j i_{0,j}\left[\exp\left(\frac{\alpha_{a,j}F}{RT}\eta_j\right) - \exp\left(-\frac{\alpha_{c,j}F}{RT}\eta_j\right)\right] \quad j = n,p \quad [3]$$

where $i_{0,j}$ is the concentration dependent equilibrium exchange current density at an interface and is given by

$$i_{0,j} = k_j(c_{1,j}^{\max} - c_{1,j}^{s})^{\alpha_{a,j}}(c_{1,j}^{s})^{\alpha_{c,j}}(c_2)^{\alpha_{a,j}} \quad j = n,p \quad [4]$$

The overpotential for the Li-ion intercalation reaction was given by

$$\eta_j = \phi_1 - \phi_2 - U_{j,\text{ref}} - \frac{J}{a_n}R_{\text{film}} \quad j = n,p \quad [5]$$

The equilibrium potentials ($U_{j,\text{ref}}$) of positive and negative electrode are expressed as functions of state-of-charge (SOC)

$$U_p^{\text{ref}} \rightarrow \text{fn}(\theta)$$
$$U_n^{\text{ref}} \rightarrow \text{fn}(\theta) \quad [6]$$

where θ is the SOC of the electrode. The empirical expressions for equilibrium electrode potentials as functions of SOC are given in Appendix A, Eq. A1, A2. For the quantitative description of electrochemical Li intercalation/deintercalation into Li-insertion electrodes, Frumkin intercalation isotherm can also be adopted as explained by Levi *et al.*[16] However, only empirical expressions were used in this paper to represent equilibrium potentials of positive and negative electrodes as a function of SOC. The term R_{film} in Eq. 5 represents the film resistance developed as a result of solvent reduction reaction that takes place during charging of Li-ion cell.

BV kinetics for the solvent reduction reaction.—Similar to Li-ion intercalation reaction, BV kinetic expression was used to explain the rate of solvent reduction (Eq. 1) as

$$J_s = i_{os}a_n\left\{\left(\frac{C_P}{C_P^*}\right)e^{(\alpha_a nf\eta_s)} - \left(\frac{C_S}{C_S^*}\right)\left(\frac{C_{Li^+}}{C_{Li^+}^*}\right)^2 e^{(-\alpha_c nf\eta_s)}\right\} \quad [7]$$

While including the side reaction along with the intercalation reaction, some approximations were made to simplify the calculations and hence the model. The kinetic expression (Eq. 7) can be reduced to either a Tafel or linear approximation depending on the reaction conditions. The cathodic Tafel approximation could be used if the solvent reduction reaction is considered to be irreversible. Thus the rate expression for the side reaction becomes

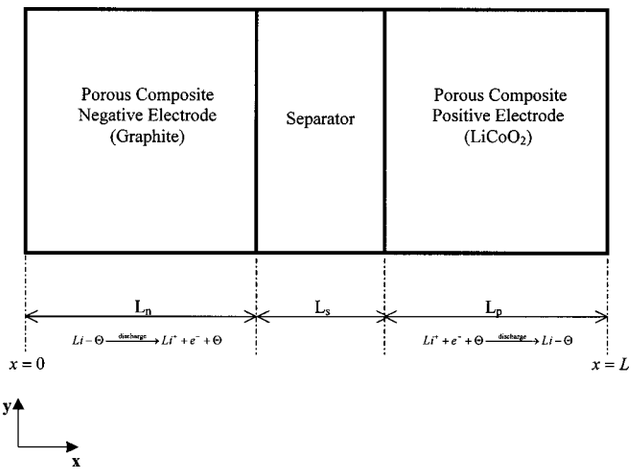

Figure 1. Schematic of a typical Li-ion cell sandwich.

$$J_s = -i_{os}a_n\left(\frac{C_S}{C_S^*}\right)\left(\frac{C_{Li^+}}{C_{Li^+}^*}\right)^2 e^{(-\alpha_c nf\eta_s)} \quad [8]$$

There may not be much variation in the concentration of Li ions in solution for low to moderate rates of charge and discharge. Moreover, solution phase Li-ion concentration as well as the solvent concentration may not be limiting for the side reaction to take place, as they will be present in excess. Based on these assumptions, the cathodic Tafel kinetics developed for the side reaction can still be simplified by not considering the concentration dependencies. Thus the rate expression can be represented as

$$J_s = -i_{os}a_n e^{(-\alpha_c nf\eta_s)} \quad [9]$$

where the overpotential term η_s is expressed as

$$\eta_s = \phi_1 - \phi_2 - U\text{ref}_s - \frac{J}{a_n}R_{\text{film}} \quad [10]$$

As mentioned earlier in the assumption, $U\text{ref}_s$ was taken as 0.4 V *vs.* Li/Li^{+}. For the first cycle, the film resistance, R_{film}, is defined as

$$R_{\text{film}} = R_{\text{SEI}} + R_P(t) \quad [11]$$

where R_{SEI} refers to the resistance of the SEI layer formed initially during the formation period and $R_P(t)$ is the resistance of the products formed during charging and is defined by

$$R_P(t) = \frac{\delta_{\text{film}}}{\kappa_P} \quad [12]$$

and the rate at which the film thickness increases is given by

$$\frac{\partial\delta_{\text{film}}}{\partial t} = -\frac{J_s M_P}{a_n\rho_P F} \quad [13]$$

Thus for any cycle number N, the film resistance is given by

$$R_{\text{film}}|_N = R_{\text{film}}|_{N-1} + R_P(t)|_N \quad [14]$$

Model Equations

Figure 1 shows a schematic representation of a typical Li-ion cell consisting of three regions namely negative electrode (graphite), separator (poly-propylene) and positive electrode ($LiCoO_2$). Both the graphite and $LiCoO_2$ are porous composite insertion electrodes. A Li-ion intercalation model[12] was used as a basis for developing this capacity fade model. The model equations, initial, and boundary

conditions that describe the mass transport, and charge transport of Li-ions in both solid and solution phases are summarized in Appendix B, Eq. B-1 to B-17 and are discussed in detail in Ref. 12, 13 and 17.

For incorporating the solvent reduction reaction, the following additional model equations have been added to the existing Li-ion model.

1. The mass transport of Li-ion inside the particle has been represented by means of spherical diffusion equation for both positive and negative electrode. At the surface of the negative electrode, as a result of side reaction, the boundary condition was modified as

$$r = r_n \quad -D_n^s \frac{\partial c_{1,n}}{\partial r} = \frac{J_I}{a_n F} \qquad [15]$$

because a part of applied current (J_s) is utilized for the solvent reduction reaction.

2. For calculating the total charge capacity available from the positive electrode after a complete constant current and constant voltage (CC-CV) charging for any cycle, the following equation has been used

$$Q_P = \int_0^{t=T_{CC+CV}} \varepsilon_p \sigma_p \left.\frac{\partial \phi_1}{\partial x}\right|_{x=L_p} dt \qquad [16]$$

3. For the estimation of capacity lost as a result of side reaction at the negative electrode surface, the following equation has been used

$$Q_s = -\int_0^{t=T_{CC+CV}} i_s dt \qquad [17]$$

where the term i_s refers to the current due to the side reaction integrated across the length of the negative electrode

$$i_s = \int_0^{L_n} J_s dx \qquad [18]$$

4. At the end of every charge cycle, the total capacity lost as a result of side reaction is estimated based on Eq. 17, which is followed by calculation of loss of SOC as follows

$$\theta_l = \frac{Q_s}{Q_{max}} \qquad [19]$$

In the above equation, Q_{max} is the initial rated capacity of the cell. For simulating the capacity in the next charge cycle, the SOC of the positive electrode has to be updated and hence the general initial condition for SOC of cathode for any cycle number (N) is given by

$$\theta_p^o|_N = \theta_p^o|_{N-1} - \theta_l|_{N-1} \qquad [20]$$

In the above expression, it is assumed that although capacity loss occurs only at the negative electrode, it causes the capacity of the positive electrode to diminish by the same magnitude.

As a result of side reaction, the film resistance over the surface of the negative electrode continues to increase during both constant current and constant voltage charging. Hence, an average value of film resistance calculated over the entire length of negative electrode was chosen as initial condition for the next cycle. The decrease in the charge capacity available from positive electrode (Q_p) is the capacity fade of the battery with cycling.

The design adjustable parameters for positive and negative electrodes are presented in Table I. The parameters for the solvent reduction reaction are given in Table II. The set of eight independent governing equations for eight dependent variables (c_1, c_2, ϕ_1, ϕ_2, J_1, J_s, Q_s, and Q_p) are solved as a 1D-2D coupled model for the three domains (negative/separator/positive) using FemLab software.

Table I. Electrode parameters for intercalation model.

Symbol	Units	Anode (graphite)	Cathode ($LiCoO_2$)
L_i	μm	88	80
σ	S/m	100	100
ε_1		0.49	0.59
ε_2		0.485	0.385
brug		4	4
δ	μm	2	2
c_1^{max}	mol/m^3	30555	51555
θ^0		0.03	0.95
D_1	m^2/s	3.9×10^{-14}	1.0×10^{-14}
k	A/m^2/(mol/m^3)$^{3/2}$	4.854×10^{-6}	2.252×10^{-6}
α_a		0.5	0.5
α_c		0.5	0.5
c_2^0	mol/m^3	1000	
D_2	m^2/s	7.5×10^{-10}	
t^+		0.363	
R_{SEI}	Ω m^2	0.01	0

Results and Discussions

Simulation of charge characteristics.—The capacity fade model was set to run under normal cycling conditions with constant current charging till the cell voltage reached 4.2 V followed by constant voltage charging until the charging current dropped to 50 mA. Thus the negative electrode potential ($\phi_2 - \phi_1$) at the current collector end never reached 0 V or less and hence, a lithium deposition side reaction was not considered for this model.

Figure 2a and b presents simulations of the variation of cell voltage and current during CC-CV charging with cycle numbers, respectively. The cell voltage shown in Fig. 2a is the difference in the solid phase potentials (ϕ_1) between the positive ($x = L$) and negative ends ($x = 0$) of the Li-ion cell sandwich. Because ϕ_1 was set to zero at $x = 0$, the solid phase potential at the positive end ($\phi_1|_{x=L}$) is the cell voltage. The applied current during both constant current and constant voltage charging was estimated using Ohm's law given by

$$i_{app} = \varepsilon_p \sigma_p \left.\frac{\partial \phi_1}{\partial x}\right|_{x=L} \qquad [21]$$

As shown in Fig. 2b, the model predicts a decrease in CC charging time and increase of the CV charging time as a function of cycle number. The model results indicated that a gradual decrease in total charging time occurs with cycling. This phenomenon was also observed experimentally.[15] As a result of the side reaction, the film resistance continued to increase with cycling, which reduced the constant current charging time due to continuous increase of the voltage drop at the interface. The SOC of the cathode material decreased for each cycle (Eq. 19, 20), which also contributes the cell voltage to reach the cutoff value earlier resulting in a decrease in total charging time with cycling.

Figure 3 presents the simulated charge curves that show the decrease in the capacity with cycling. This includes both constant cur-

Table II. Parameters for the solvent reduction side reaction.

Symbol	Units	Value
$U\text{ref}_s$	V	0.4
M_P	mol/kg	7.3×10^4
ρ_P	kg/m^3	2.1×10^3
i_{os}	A/m^2	1.5×10^{-6}
κ_P	S/m	1

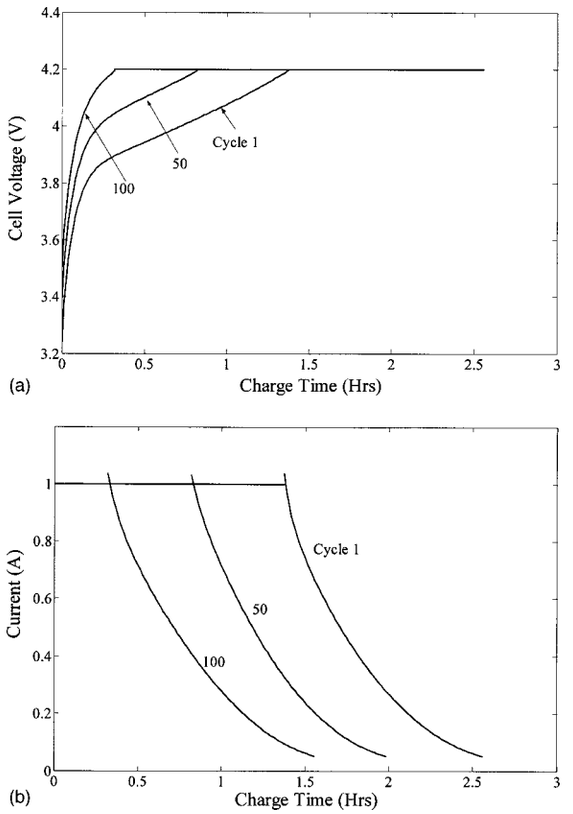

Figure 2. (a) Variation of cell voltage during CC-CV charging for various cycles. (b) Variation of current during CC-CV charging for various cycles.

rent and constant voltage parts of the charge cycle and the capacity was calculated using Eq. 16. During the CC part, the current was constant and the capacity was obtained by the product of current and charge time. During the CV part, the current decayed during charge as shown in Fig. 2b. Hence, the capacity was calculated using Eq. 16. The SOC was corrected at the end of each cycle by using Eq. 20, which accounts for the capacity loss due to the side reaction.

Simulation of discharge characteristics.—Figure 4 shows the simulated discharge curves after 1, 50, and 100 cycles. Due to the loss of the active material as a result of side reaction, the SOC of the electrode material decreased while the capacity loss increased with the cycle number. Because the capacity loss due to the side reactions was assumed to occur only during charging the cell, the capacity

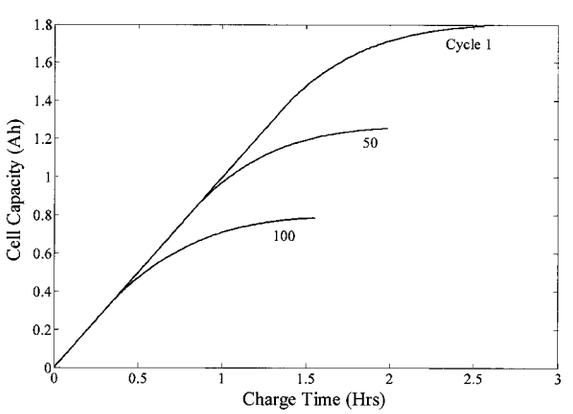

Figure 3. Charge curves of Li-ion cells for various cycles.

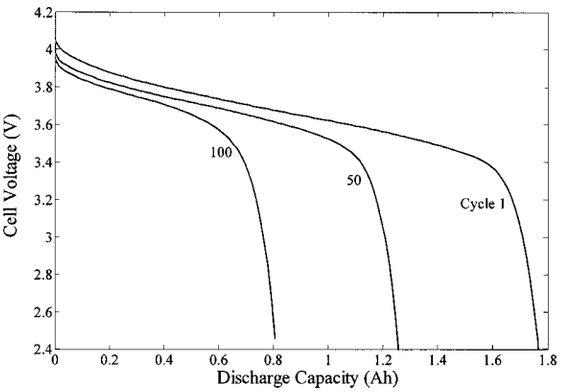

Figure 4. Discharge characteristics of Li-ion cells for various cycles.

fade model was programmed to simulate only the charging performance for every cycle. Thus, to simulate the discharge performance of the cell for any cycle number, it is necessary to run the model for the required number of charge cycles, which updates the capacity fade parameters, based on the extent of side reaction and number of cycles.

While the charge simulation was in progress, the parameter values contributing to the cell capacity loss and the cell voltage drop could be collected at the end of every cycle. Thus, to estimate the discharge performance after any cycle number, the Li-ion intercalation model could be run only once with the updated parameters. Apart from the capacity loss with continued cycling simulations, the voltage plateau of simulated discharge curves continued to decrease which is attributed to the continuous increase in the film resistance during charging as a result of the side reaction.

The variation of film resistance over the particle surface of negative electrode has been shown in Fig. 5. the solid line of Fig. 5 (top *x* axis and right *y* axis) presents the increase in the film resistance during CC-CV charging estimated for cycle number 40 by using Eq. 12, 13. The dotted line of Fig. 5 (bottom *x* axis and left *y* axis) presents the variation of film resistance with cycling which increased almost linearly with increase in cycle number. The film resistance after any charge cycle was calculated using Eq. 14. Thus as shown in Fig. 5, due to the side Reaction 1, the film resistance continuously increased with cycling thereby causing an increased drop in the voltage plateau in the simulated discharge curves.

Capacity fade with cycling.—The variations of cell capacity (Q_p) with number of cycles, capacity lost per cycle (Q_s), and the SOC lost per cycle (θ_l) are shown in Fig. 6. Since in the model, the capacity loss was assumed to occur only during charging, the de-

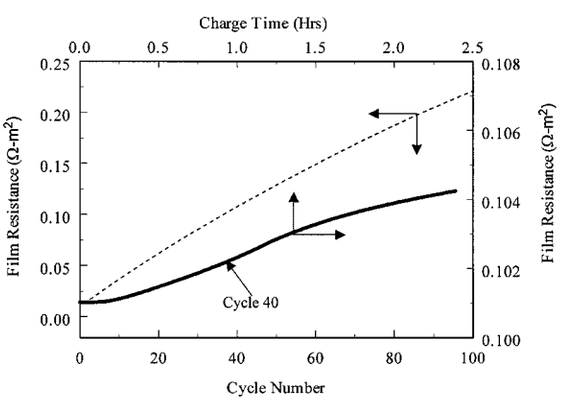

Figure 5. Variation of film resistance during charging for (solid line) cycle 40 and (dotted lines) variation of film resistance with cycle number.

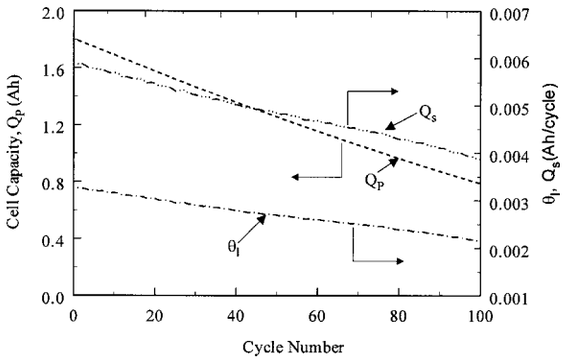

Figure 6. Variation of cell capacity (Q_P), capacity loss per cycle (Q_s), and SOC loss per cycle (θ_l) with cycle number.

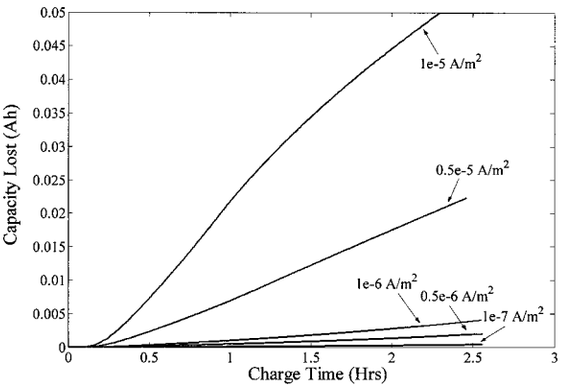

Figure 7. Effect of i_{os} over capacity loss with charging.

crease in the capacity of the cell (Q_P) after every charge cycle corresponded to the actual capacity fade of the cell. Both the cell capacity and the capacity loss per cycle decreased linearly with increase in cycle number. Both these effects have been observed experimentally.[18] An interesting result from the model simulations is the decrease in capacity loss per cycle (Q_s) during continuous cycling. This indicates that the active material loss due to the side reaction is more pronounced during initial phases of cycling and becomes progressively lower with cycling. SEI formation at the carbon particle surface does not stop with the first cycle but continues during initial charge/discharge cycles. With time, the film formation becomes more stable in nature and leads to lower capacity fade per cycle (Q_s) as seen in Fig. 6. The SOC of the electrode material also decreased with cycling as described in Eq. 19 and 20.

Case Studies

The discussions given above were primarily focused on the capacity fade simulations for fixed values of adjustable parameters, which control the capacity loss and the film resistance. The charge simulations were carried out from a completely discharged state (100% depth of discharge, DOD). The case studies discussed below include the effect of parameters that control the side reactions namely the exchange current density (i_{os}), the film conductivity (κ_P), and the influence of cycling conditions such as end of charge voltage (EOCV) and the DOD over capacity fade.

Effect of i_{os} and κ_P on capacity fade.—For all simulations discussed above, both i_{os} and κ_P were assumed. In order to match the simulated charge and discharge performance with the experimental cycling data, it would be critical to estimate the capacity fade parameters by using a nonlinear parameter estimation method. The initial values of the parameters could be chosen to fit the first cycle and with the experimental data of consecutive cycles, the parameter values has to be estimated to obtain a better fit which will be used as initial guesses for the next cycle and so on. Because the objectives of this study were to identify the right parameters which control the capacity fade through first principles and to study the effect of the parameters over capacity loss under different cycling conditions, no attempt was made to estimate the right values for the parameters or to fit the simulated results to experimental data.

Figure 7 shows the effect of exchange current density for side reaction (i_{os}) over capacity loss (Q_s) during charging. The simulations correspond to the first charge cycle for all values of i_{os}. It is clear from the plot that increasing the value of i_{os} by even one order of magnitude dramatically increased the capacity loss with charging. By increasing i_{os}, the rate of the side reaction increased and hence the capacity lost during charging (Q_s), was higher at higher rates. Similar simulations were done to analyze the effect of conductivity of the products formed over the film resistance $R_P(t)$, and it was found that less conductive products formed during the side reaction would increase the film resistance dramatically.

Effect of EOCV on capacity fade.—The most significant variables that are widely considered to control the cycle life of Li-ion cells are the EOCV and the DOD. One of the reasons for capacity fade in Li-ion cells is overcharging the cell. Overcharging the lithium-ion cells can result in safety concerns if the voltage is allowed to rise above 4.3 V per cell. Cell manufacturers usually suggest charging to 4.2 V to obtain a maximum capacity from the cell.

Li-ion batteries become increasingly unstable if charged to higher voltages. Overcharging the cell by 0.1 V will not only result in safety issues but also can reduce cycle life by up to 60%.[19] The capacity fade model could be used as a predictive tool for cycling performance of Li-ion cells when charged to different end potentials.

Figure 8 presents the variation of current during CC-CV charging for cycle number 10, where the model was simulated for three different end potentials namely 3.9, 4.0, and 4.2 V. Since the model takes less time to reach lower cutoff potentials, the CC charging time are lower for cells charged to 3.9 and 4.1 V when compared with those charged to 4.2 V. The percentage CC times for different EOCV simulations are found to be 9.3, 21.8, and 51.4% for 3.9, 4.0, and 4.2 V, respectively.

In order to reach the rated capacity, the Li-ion cell has to be charged in constant current mode until the voltage reaches 4.2 V followed by float charging at 4.2 V until the charging current drops to a very low value of approximately C/100 rate. For cut-off potentials lower than 4.2 V, the cells are always partially charged depending on the EOCV chosen. The same phenomenon was observed in the simulations presented in Fig. 9, which show the variations of the charge capacity for different EOCVs. The dotted lines in the figure separate the capacity obtained from CC and CV charging for each case.

The capacity loss during CC-CV charging and the overpotential for side reaction for cells charged to different EOCV is shown in Fig. 10. The overpotential for side reaction (η_s) was calculated using Eq. 10 at the negative electrode end ($x = 0$) and the capacity loss (Q_s) was estimated using Eq. 17. As expected, the capacity loss increased by increasing the cutoff potentials. In other words, the overpotential for side reaction (η_s) became more negative by increasing the EOCVs. Increase of the overvoltage resulted in an increase of the capacity loss.

Figure 11 presents the cycling simulations for different EOCVs. Based on simulation results for 10 cycles, it was found for all cases that the capacity continued to decrease with cycling. However capacity decrease was found to be higher for 4.2 V when compared with the other EOC potentials.

The capacity fade of Li-ion cells that were cycled with different EOC voltages were calculated through periodic capacity measurement where the cells, irrespective of what cycling conditions used,

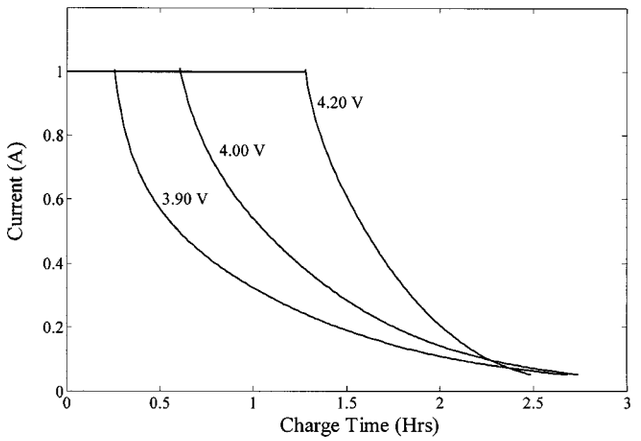

Figure 8. Variation of current during CC-CV charging for the cells charged to different EOCV.

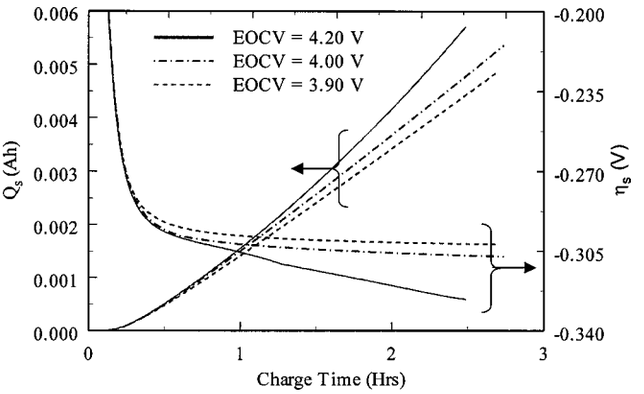

Figure 10. Comparison of capacity loss (Q_s) with charging and variation of overpotential for side reaction (η_s) for Li-ion cells charged to different EOCV.

were allowed to charge in CC mode till the cell voltage reached 4.2 V followed by constant voltage charging and then a C/2 rate complete discharge. Based on the simulation results for 10 cycles, it was found that Li-ion cells that were cycled with lower cutoff potential (4.0 V and 3.9 V) suffered less capacity fade than cells cycled with an EOCV of 4.2 V. The percentage capacity fade values after 10 cycles were estimated to be 7.2, 4.4, and 3.8%, respectively, for EOCV 4.2, 4.0, and 3.9 V. This suggests that for applications where 100% of the cell capacity may not be needed, cycling the cells to lower cutoff potentials results in increased cycle life and smaller capacity loss. Also, the film resistance (R_{film}) increased with increase in EOCV due to an increased occurrence of the side reaction.

Effect of DOD on capacity fade.—DOD is defined as the level to which the battery voltage is decreased during discharge. For instance, 100% DOD means that the battery voltage decreased to the lowest level or in other words, the battery was completely discharged and 20% DOD means that 20% of the battery capacity has been removed. This level of DOD is often referred to as a shallow discharge. The shallower the discharge, the more cycles the battery will provide. The capacity fade model can be used to simulate the cycling performance of Li-ion cells as a function of DOD.

In this case study, the EOCV was set at 4.2 V and DOD chosen were 20, 40, and 60%, and the results were compared with those obtained for 100% DOD. The SOC of the positive and negative electrodes corresponding to the different DODs was estimated by running the intercalation model once. These SOCs were used as initial conditions for cycling simulations. After 10 cycles, capacity check simulations were done for all DODs. Figure 12 summarizes the simulated charge curves for different DODs for the first cycle. The constant current charging time decreased for the cells charged from lower depth of discharge namely 20 and 40% when compared with 60 and 100%. The percentage CC times for different DOD simulations are found to be 8.3, 25.2, 36.6, and 53.8% for 20, 40, 60, and 100 DOD, respectively. Thus most of the capacity was obtained during constant voltage charging for cells in shallow discharged state.

Since the total charging time is lower for the cells charged from partially discharge state, the capacity loss as a result of side reaction would also be smaller when compared with charging from a completely discharged state. Figure 13 shows the variation of SOC of positive electrode for cycling under different DOD.

Figure 14 presents the simulations of capacity loss during charging for different DOD. The rate at which the capacity loss increase with cycling was observed to be more steep for cells discharged from 60 and 100% DOD. After 10 cycling simulations for each DOD, a capacity check has been performed for each DOD and the capacity fade was estimated to be 3.5, 4.9, 6.1, and 7.2% for 20, 40, 60, and 100% DOD, respectively. Thus cells charged from shallow discharge loose less SOC and hence capacity and provide more cycles and longer life.

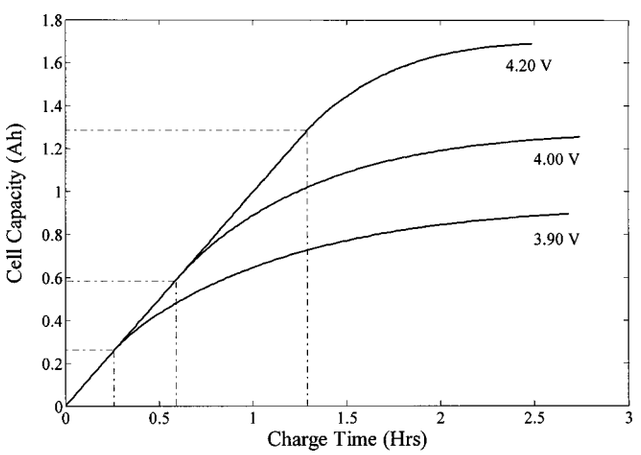

Figure 9. Variation of charge capacity after the 10th cycle when the cells were charged to different EOCV.

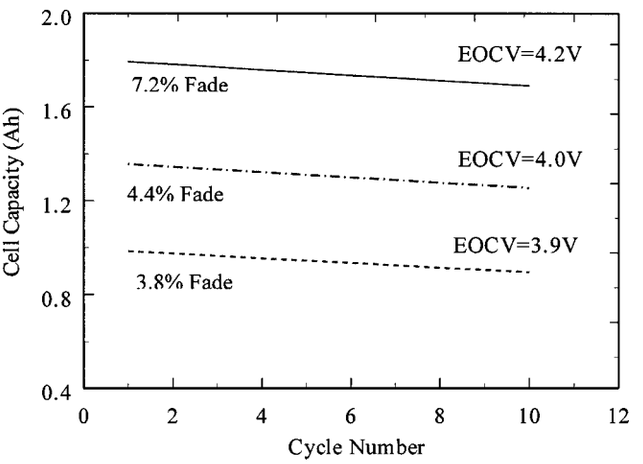

Figure 11. Variation of cell capacity with cycling when the cells were charged to different EOCV.

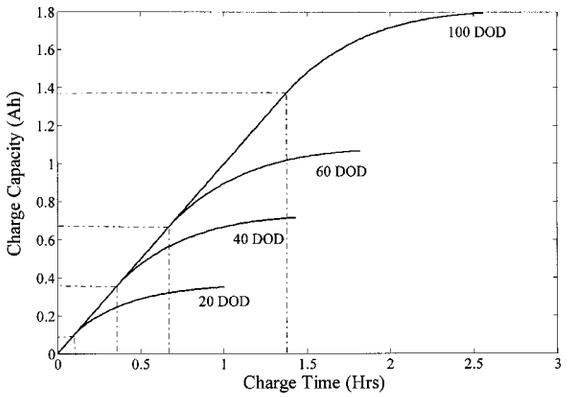

Figure 12. Charge curves Li-ions for the first cycle when charged from different DOD.

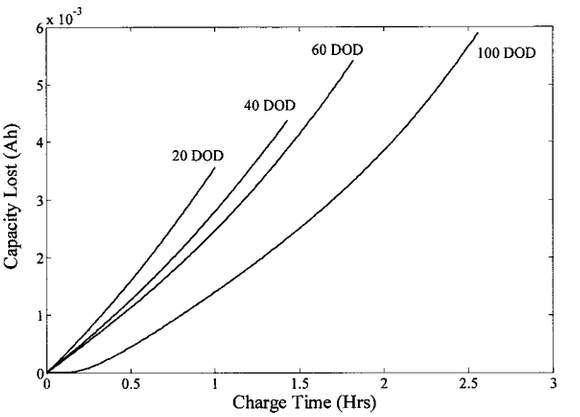

Figure 14. Variation of capacity loss during charging for the cells charged from different DOD.

The capacity fade model developed based on first principles was capable of simulating the cycling performance of Li-ion cells. The model predicted the performance of the cell under several cycling conditions such as charging to several cutoff values and charging from several DOD. The model was also capable of explaining higher capacity loss for cells cycled at elevated temperatures because the rate of the side reaction would be higher at high temperatures. Abuse conditions such as overcharge can lead to film formation from the deposition of metallic lithium onto the negative electrode. Any lithium metal formed in the cell will probably undergo secondary reactions leading to more thick reaction product layers or secondary films. Incorporation of lithium deposition reaction to the existing capacity fade model will thus predict the cycling performance under overcharging conditions.

Conclusions

The capacity fade model developed and discussed in this paper could be used as a basis for predicting the cycle life and analyzing the discharge characteristics of Li-ion cells after any cycle number. The effect of parameters (EOCV and DOD, the film resistance, the exchange current density and the overvoltage of the parasitic reaction) was studied qualitatively. The next step involves estimation of these time-dependent parameters based on the initial cycling data obtained experimentally. More than one mechanism could also be incorporated in the model to explain the capacity loss. The model developed assumes that the entire capacity loss was due to the side reaction over the surface of negative electrode during CC-CV charging. Other reactions such as electrolyte oxidation and phase transformation etc., that are specific to electrode materials could also be included in the capacity fade model for better predictions.

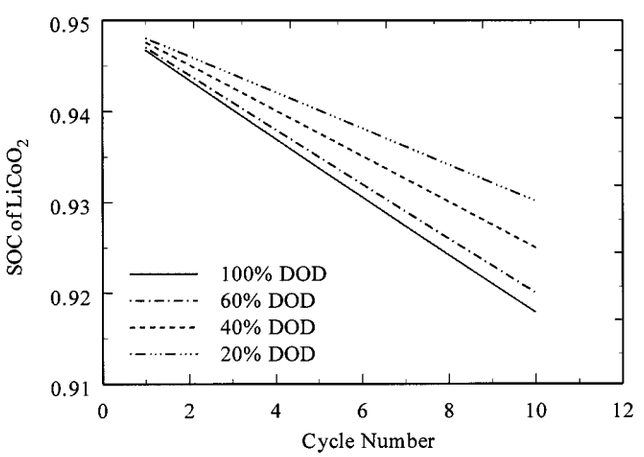

Figure 13. Variation of SOC of $LiCoO_2$ with cycle number for the cells cycled from different DOD.

Acknowledgment

Financial support provided by National Reconnaissance Office for Hybrid Advanced Power Sources no. NRO-00-C-1034 is acknowledged gratefully.

The University of South Carolina assisted in meeting the publication costs of this article.

Appendix A

For the graphite electrode

$$U_n^{\text{ref}} = 0.7222 + 0.1387\theta_n + 0.029\theta_n^{1/2} - \frac{0.0172}{\theta_n} + \frac{0.0019}{\theta_n^{1.5}} + 0.2808e^{(0.90-15\theta_n)} - 0.7984e^{(0.4465\theta_n-0.4108)} \quad [A\text{-}1]$$

For the $LiCoO_2$ electrode

$$U_p^{\text{ref}} = \frac{-4.656 + 88.669\theta_p^2 - 401.119\theta_p^4 + 342.909\theta_p^6 - 462.471\theta_p^8 + 433.434\theta_p^{10}}{-1 + 18.933\theta_p^2 - 79.532\theta_p^4 + 37.311\theta_p^6 - 73.083\theta_p^8 + 95.96\theta_p^{10}} \quad [A\text{-}2]$$

Appendix B

The governing equations for potential distribution in solid and solution phases were

$$\nabla \cdot (\sigma^{\text{eff}}\nabla\phi_1) - J = 0 \quad [B\text{-}1]$$

$$\nabla \cdot (\kappa^{\text{eff}}\nabla\phi_2) + \nabla \cdot (\kappa_D\nabla \ln c_2) + J = 0 \quad [B\text{-}2]$$

respectively, where the effective conductivities are given by Bruggeman's correlation given by

$$\sigma_j^{\text{eff}} = \sigma_j\varepsilon_{1,j} \quad j = n,p \quad [B\text{-}3]$$

$$\kappa^{\text{eff}} = \kappa\varepsilon_2^{\text{brug}} \quad [B\text{-}4]$$

and the diffusional conductivity (κ_D) is given by

$$\kappa_D = \frac{2RT\kappa^{\text{eff}}(\tau - 1)}{F} \quad [B\text{-}5]$$

for constant values of transference number and solution phase diffusivity at all times and at all points in the cell.

The solution phase conductivity as a function of concentration c_2 (in mol/dm^3) is[20]

$$\kappa^{\text{eff}} = \kappa\varepsilon_2^{4.0} = \begin{pmatrix} 4.1253 \times 10^{-4} + 5.007c_2 - 4.7212 \times 10^3c_2^2 \\ +1.5094 \times 10^6c_2^3 - 1.6018 \times 10^8c_2^4 \end{pmatrix}\varepsilon_2^{4.0} \quad [B\text{-}6]$$

The model equation that describes the solid phase lithium concentration is given by

$$\frac{\partial c_{1,j}}{\partial t} = \frac{D_{1,j}}{r^2}\frac{\partial}{\partial r}\left(r^2\frac{\partial c_{1,j}}{\partial r}\right) \quad j = n,p \qquad [B\text{-}7]$$

and for explaining the mass transport of lithium ions in the solution phase the following equation used was

$$\varepsilon_2\frac{\partial c_2}{\partial t} = \nabla \cdot (D_2^{\text{eff}}\nabla c_2) + \frac{(1 - t^+)}{F}J \qquad [B\text{-}8]$$

where the effective diffusivity D_2^{eff} of the solution phase is given by

$$D_2^{\text{eff}} = D_2\varepsilon_2^{\text{brug}} \qquad [B\text{-}9]$$

Initial condition

$$c_{1,j} = c_{1,j}^0 \text{ and } c_2 = c_2^0 \text{ at } t = 0 \text{ for all } x \geqslant 0 \qquad [B\text{-}10]$$

Boundary and interface conditions
BC for solid phase potential (ϕ_1)

$$\text{At } x = 0, \quad \phi_1 = 0 \qquad [B\text{-}11]$$

$$\text{AT } x = L, \quad -\sigma_p^{\text{eff}}\frac{\partial\phi_1}{\partial x} = i_{\text{app}} \qquad [B\text{-}12]$$

BC for solution phase potential (ϕ_2)

$$\text{At } x = 0 \text{ and } x = L, \quad \kappa\frac{\partial\phi_2}{\partial x} + \kappa_D\frac{\partial \ln c_2}{\partial x} = 0 \qquad [B\text{-}13]$$

BC for solution phase concentration (c_2)

$$\text{At } x = 0 \text{ and } x = L, \quad \frac{\partial c_2}{\partial x} = 0 \qquad [B\text{-}14]$$

Boundary conditions at the interfaces for ϕ_1, ϕ_2, and c_2
For ϕ_1

$$\text{at } x = L_{n,s}, \quad \left.\frac{\partial\phi_1}{\partial x}\right|_- = 0 \qquad [B\text{-}15]$$

$$\text{at } x = L_{s,p}, \quad \left.\frac{\partial\phi_1}{\partial x}\right|_+ = 0 \qquad [B\text{-}16]$$

For ϕ_2 and c_2, at all the interfaces, all fluxes on the left of the interface are equated to those on the right.
BC for solid phase concentration

$$\text{at } r = 0, \quad \frac{\partial c_{1,j}}{\partial r} = 0, \quad j = n,p \qquad [B\text{-}17]$$

List of Symbols

A	specific surface area of porous electrode, m^2/m^3
C	concentration of Li or Li^+ ions, mol/m^3
cyc	charge-discharge cycle
D	diffusion coefficient, m^2/s
F	Faraday's constant, 96487 C/mol
i_0	exchange-current density for intercalation reaction, A/m^2
i_{os}	exchange-current density for side reaction, A/m^2
i_{app}	applied current density, 16.54 A/m^2
J_I	local volumetric current density for intercalation reaction, A/m^3
J_s	local volumetric current density for side reaction, A/m^3
k	rate constant of electrochemical reaction, $A/m^2/(mol/m^3)^{1+\alpha_a}$
L	length of the cell, m
M	molecular weight, mol/kg
Q_p	capacity of the positive electrode, A h
Q_s	capacity lost due to side reaction, A h
R	particle radius, μm
R_{film}	film resistance at the electrode/electrolyte interface, $\Omega\ m^2$
R_p	resistance of the film products, $\Omega\ m^2$
R_g	universal gas constant, 8.314 J/mol
r	radial coordinate, m
T	temperature, K
t	time, s
U	local equilibrium potential, V
V	cell voltage, V
X	coordinate across the cell thickness, m

Greek

α_a, α_c	anodic and cathodic transfer coefficients of electrochemical reaction
ε	volume fraction of a phase
ϕ	local potential of a phase, V
η	local over potential driving electrochemical reaction, V
κ	conductivity of electrolyte, S/m
θ	state-of-charge
σ	conductivity of electrode, S/m
ρ	density of active material, kg/m^3
δ	film thickness, m

Subscript

1	solid phase
2	solution phase
n	negative electrode
N	cycle number
p	positive electrode
P	product formed due to side reaction
ref	reference
−	to the left of an interface
+	to the right of an interface

Superscript

0	initial
Li/Li^+	relative to Li/Li^+ reference
max	theoretical maximum

References

1. R. Darling and J. Newman, *J. Electrochem. Soc.*, **145**, 990 (1998).
2. R. Spotnitz, *J. Power Sources*, **113**, 72 (2002).
3. P. Arora, R. E. White, and M. Doyle, *J. Electrochem. Soc.*, **145**, 3647 (1998).
4. P. Ramadass, Bala S. Haran, R. White, and B. N. Popov, Abstract 33, The Electrochemical Society Meeting Abstracts, Vol. 2002-2, Salt Lake City, UT, Oct 20-24, 2002.
5. P. Ramadass, V. R. Subramanian, H. J. Ploehn, and R. E. White, Abstract 178, The Electrochemical Society Meeting Abstracts, Vol. 2002-2, Salt Lake City, UT, Oct 20-24, 2002.
6. O. Pensado-Rodriguez, J. R. Flores, M. Urquidi-Macdonald, and D. D. Macdonald, *J. Electrochem. Soc.*, **146**, 1326 (1999).
7. A. V. Churikov, *Electrochim. Acta*, **46**, 2415 (2001).
8. I. Nainville, A. Lemarchand, and J. P. Badiali, *Electrochim. Acta*, **41**, 2855 (1996).
9. D. Aurbach, B. Markovsky, I. Weissman, E. Levi, and Y. Ein-Eli, *Electrochim. Acta*, **45**, 67 (1999).
10. D. Aurbach, *J. Power Sources*, **89**, 206 (2000).
11. Y-G. Ryu and S-I. Pyun, *J. Electroanal. Chem.*, **433**, 97 (1997).
12. M. Doyle, T. F. Fuller, and J. Newman, *J. Electrochem. Soc.*, **140**, 1527 (1993).
13. T. F. Fuller, M. Doyle, and J. Newman, *J. Electrochem. Soc.*, **141**, 1 (1994).
14. M. D. Levi and D. Aurbach, *J. Electroanal. Chem.*, **421**, 79 (1997).
15. M. D. Levi, G. Salitra, B. Markovsky, H. Teller, D. Aurbach, U. Heider, and L. Heider, *J. Electrochem. Soc.*, **146**, 1279 (1999).
16. M. D. Levi and D. Aurbach, *Electrochim. Acta*, **45**, 165 (1999).
17. P. M. Gomadam, J. W. Weidner, R. A. Dougal, and R. E. White, *J. Power Sources*, **110**, 267 (2002).
18. P. Ramadass, B. Haran, R. White, and B. N. Popov, *J. Power Sources*, **112**, 606 (2002).
19. P. Ramadass, B. Haran, R. White, and B. Popov, *J. Power Sources*, **111**, 210 (2002).
20. M. Doyle, J. Newman, A. S. Gozdz, C. N. Schmutz, and J.-M. Tarascon, *J. Electrochem. Soc.*, **143**, 1890 (1996).